nature physics

Article

https://doi.org/10.1038/s41567-024-02635-5

The space of transport coefficients allowed by causality

Received: 11 July 2023

Accepted: 8 August 2024

Published online: 14 October 2024

Check for updates

Michal P. Heller[1] ✉, Alexandre Serantes[1,2], Michał Spaliński[3,4] & Benjamin Withers[5]

As an effective theory, relativistic hydrodynamics is fixed by symmetries up to a set of transport coefficients. A lot of effort has been devoted to explicit calculations of these coefficients. Here we adopt a more general approach, deploying bootstrap techniques to rule out theories that are inconsistent with microscopic causality. What remains is a universal convex geometry in the space of transport coefficients, which we call the hydrohedron. The landscape of all consistent theories necessarily lies inside or on the edges of the hydrohedron. We analytically construct cross-sections of the hydrohedron corresponding to bounds on transport coefficients that appear in sound and diffusion modes' dispersion relations for theories without stochastic fluctuations.

Hydrodynamics is a universal description of systems tending towards thermal equilibrium. It is formulated as an effective theory, order by order in a gradient expansion, which at the classical linearized level can be mapped to the expansion of the mode frequencies ω in powers of the wave-vector k:

$$\omega(k) = \sum_{n=1}^{\infty} c_n k^n. \tag{1}$$

Such hydrodynamic Taylor series expansions have been studied in a wide variety of examples and have been found to have a finite radius of convergence[1–6]. The complex c_n are a collection of transport coefficients that include the speed of sound and the diffusion constant. The aim of this paper is to characterize the set of physically acceptable collections of transport coefficients, which can be thought of as the landscape of hydrodynamic theories. We propose to chart its boundaries by imposing the causality condition[7]

$$v_{\mathrm{LC}}\,|\mathfrak{Im}\,k| - \mathfrak{Im}\,\omega(k) \geq 0. \tag{2}$$

where v_{LC} is the lightcone speed (we set $v_{\mathrm{LC}} = 1$ in what follows). This condition arises axiomatically, a consequence of position space retarded Green's functions being tempered distributions and causality dictating support only in the appropriate lightcone. This implies that certain regions of its Fourier transform are analytic, thus restricting where physical modes can appear. In ref. 7, we used equation (2) to prove that all dissipative hydrodynamic expansions (equation (1)) have a finite radius of convergence R and establish two-sided bounds on all dimensionless combinations $R^{n-1}c_n$.

In the present work, we propose to view equation (2) in a completely new way. Taking only the minimal ingredients of analyticity of the mode functions at $k = 0$ (equation (1)) and the causality of the Green's function in equation (2), we seek to constrain where the landscape of admissible transport coefficients lies. This strategy adheres to the bootstrap approach to theoretical physics problems, which carves out a space of consistent theories using fundamental principles. It also enables us to profit from technologies used in other such programmes such as the modern conformal bootstrap[8–11] and the S-matrix bootstrap (for example, refs. 12–16).

In particular, the two-sided bounds on all $R^{n-1}c_n$ from ref. 7 tell us already that the landscape lies inside an infinite-dimensional hypercube. Utilizing the tools surrounding positive moments, detailed in ref. 17 (see also refs. 18,19), we cleave away excluded regions from the hypercube, so as to characterize more precisely the physically relevant region enclosed within. We refer to the region that remains at the end of this cleaving process as the hydrohedron. Given the minimal set of

[1]Department of Physics and Astronomy, Ghent University, Ghent, Belgium. [2]Departament de Física Quàntica i Astrofísica, Institut de Ciències del Cosmos (ICCUB), Facultat de Física, Universitat de Barcelona, Barcelona, Spain. [3]Physics Department, University of Białystok, Białystok, Poland. [4]National Center for Nuclear Research, Warszawa, Poland. [5]Mathematical Sciences and STAG Research Centre, University of Southampton, Highfield, Southampton, UK. ✉e-mail: michal.p.heller@ugent.be

assumptions that went into this process, the resulting geometry is otherwise completely universal, independent of, for example, spacetime dimension, state or microscopic theory under consideration.

The hydrohedron has cross-sections of special physical significance. We will consider two examples in detail, corresponding to diffusive and sound modes. We will refer to them as the diffusion cross-section and the sound cross-section, respectively. In the diffusion cross-section, coefficients of odd powers of k in equation (1) are set to zero, whereas coefficients of even powers are purely imaginary. In the sound cross-section, coefficients of odd powers of k in equation (1) are purely real, whereas coefficients even powers are purely imaginary.

The natural scale of the problem

With the exception of c_1, the transport coefficients appearing in equation (1) are dimensionful parameters. It is conventional to normalize these parameters by thermodynamic quantities, such as appropriate powers of temperature. In the special case of the shear-viscosity η (which appears in $\Im\mathfrak{m}\, c_2$), the dimensionless combination η/s is often considered, where s is the entropy density. The Kovtun–Son–Starinets (KSS) bound $\frac{\eta}{s} \geq \frac{1}{4\pi}$ (ref. 20) is naturally expressed in this way.

However, in stark contrast, imposing causality (equation (2)) gives rise to bounds on transport coefficients normalized by R, the radius of convergence of the hydrodynamic series (equation (1)), as our results below demonstrate. Roughly speaking, R arises because equation (2) is utilized by integrating within a disk centred on $k = 0$, and the strongest constraint is given by the largest disk possible for which the function is still analytic: that is, a disk of radius R. The hydrohedron geometry then lives in the space spanned by the dimensionless transport coefficients, $\{R^{n-1}c_n\}$.

For example, in the case of a shear mode in a conformal theory, $c_2 = -\mathrm{i}\frac{\eta}{\epsilon+P}$ with ϵ being the energy density and P the pressure, we find bounds on the dimensionless combination $R\eta/(\epsilon+P)$. Firstly we find two-sided bounds on $R\eta/(\epsilon+P)$ alone, and then we find an infinite set of bounds that relate $R\eta/(\epsilon+P)$ to other dimensionless transport combinations, $R^{n-1}c_n$. Note that we do not bound the combination η/s directly; see also the discussion around equation (22).

We stress that R is not a formal or abstract quantity. Given a microscopic theory (or a sufficient number of terms of the hydrodynamic gradient expansion), it is computable, and it is also in principle measurable in experiment. Indeed, R has already been computed in a variety of holographic theories as well as kinetic theory; see ref. 6 for a discussion. For example, for the $\mathcal{N} = 4$ supersymmetric Yang–Mills (SYM) theory at finite temperature and chemical potential μ, a holographic computation gives $R = (\epsilon + P)/(2\mu\sqrt{\eta})$ for a numerically known range of μ (refs. 1,5). In general, the value of R varies across theories or spatial dimensions or within a given theory as the temperature or other thermodynamic parameters are varied. Additionally, R is a natural quantity from an effective field theory point of view; as the radius of convergence of equation (1), it marks the precise point at which non-hydrodynamic degrees of freedom become important. This is because R is set by branch point singularities corresponding to other modes[7]. In other words, R is the natural effective field theory cutoff scale for hydrodynamics. Note that the explicit presence of the ultraviolet cutoff in effective field theory bounds should not come as a surprise; see for example ref. 21.

The diffusion cross-section

As mentioned earlier, in this paper we will restrict our analysis to two cross-sections of the full hydrohedron of particular physical significance. We start in this section by specializing to a diffusive mode: that is, a dispersion relation of the form

$$\omega(k) = \mathrm{i}\sum_{n=1}^{\infty}\beta_{2n}k^{2n}, \tag{3}$$

where $\beta_{2n} \in \mathbb{R}$ and with a finite radius of convergence, $R > 0$. We extend k to lie in the disk of radius R centred on $k = 0$ in the complex plane, where we impose the causality condition in equation (2). Through a rigorous moment problem analysis, we derive a set of hierarchical bounds on the dimensionless coefficients $R^{2n-1}\beta_{2n}$. These bounds define a convex geometry. Full mathematical details of the analysis can found in 'Diffusion cross-section derivation'.

The first few orders in this hierarchy of bounds are given by the following expressions

$$-\frac{16}{3\pi} \leq R\beta_2 \leq 0. \tag{4}$$

$$-\frac{64}{15\pi} \leq R^3\beta_4 \leq \frac{256 - 15\pi R\beta_2\,(8 + 3\pi R\beta_2)}{90\pi}. \tag{5}$$

$$\frac{-32,768 + 1,575\pi^2\left(R\beta_2 - R^3\beta_4\right)^2 - 240\pi\left(13R\beta_2 + 14R^3\beta_4\right)}{525\pi\left(16 + 3\pi R\beta_2\right)} \leq R^5\beta_6 \leq \frac{4,096 - 525\pi^2\left(R\beta_2 + R^3\beta_4\right)^2 - 120\pi\left(31R\beta_2 + 14R^3\beta_4\right)}{175\pi\left(8 - 3\pi R\beta_2\right)}. \tag{6}$$

Note that only the dimensionless combinations $R^{2n-1}\beta_{2n}$ appear. These bounds are the first three inequalities in an infinite set. Additional inequalities arising at higher orders can be easily derived using the methods outlined in 'Diffusion cross-section derivation', and we we provide only the first three here for clarity.

Together, these define a convex geometry in the space of dimensionless transport coefficients $\{R^{2n-1}\beta_{2n}\}$. Because we have restricted our analysis here to diffusive modes (equation ((3)), this is a cross-section of the full hydrohedron geometry (the cross-section corresponding to setting all odd-k coefficients to zero and all even-k coefficients to be purely imaginary). These first three bounds (equations (4)–(6)) provide a projection of the diffusive cross-section of the hydrohedron to the first three transport coefficients, $\{R\beta_2, R^3\beta_4, R^5\beta_6\}$, a three-dimensional (3D) convex shape. This shape is illustrated in Fig. 1a.

All two-dimensional projections involving $\{R\beta_2, R^3\beta_4, R^5\beta_6\}$ are shown in Fig. 1b–d. The projection to the $(R\beta_2, R^3\beta_4)$-plane is given by the inequalities in equations (4) and (5). The other projection planes $(R\beta_2, R^5\beta_6)$ and $(R^3\beta_4, R^5\beta_6)$ are given by more complicated expressions because they also involve equation (6). For the $(R\beta_2, R^5\beta_6)$-plane, we have that the closure of the projection exists within the interval $-\frac{16}{3\pi} \leq R\beta_2 \leq 0$, with $R^5\beta_6$ upper bounded by a piecewise function

$$R^5\beta_6 \leq \begin{cases} -\frac{3,328}{945\pi} - \frac{5}{3}R\beta_2 & \\ +\pi R^2\beta_2^2 + \frac{\pi^2}{4}R^3\beta_2^3 & \text{if } -\frac{16}{3\pi} \leq R\beta_2 < -\frac{10}{3\pi} \\ \frac{136}{35\pi} & \text{if } -\frac{10}{3\pi} \leq R\beta_2 \leq 0 \end{cases} \tag{7}$$

and lower bounded by $-\frac{144}{35\pi}$. For the $(R^3\beta_4, R^5\beta_6)$-plane, the closure of the projection exists within the interval $-\frac{64}{15\pi} \leq R^3\beta_4 \leq \frac{56}{15\pi}$, with $R^5\beta_6$ upper bounded by a piecewise function

$$R^5\beta_6 \leq \begin{cases} \frac{512}{175\pi} - \frac{6}{5}R^3\beta_4 - \frac{3\pi}{8}R^6\beta_4^2 & \text{if } -\frac{64}{15\pi} \leq R^3\beta_4 < -\frac{8}{5\pi} \\ \frac{136}{35\pi} & \text{if } -\frac{8}{5\pi} \leq R^3\beta_4 < \frac{26}{15\pi} \\ \frac{\left[\begin{array}{l} -360 + 7\sqrt{30}(34 + 15\pi R^3\beta_4) \\ \times\sqrt{56 - 15\pi R^3\beta_4} \end{array}\right]}{3,150\pi} & \text{if } \frac{26}{15\pi} \leq R^3\beta_4 \leq \frac{56}{15\pi} \end{cases} \tag{8}$$

https://doi.org/10.1038/s41567-024-02635-5

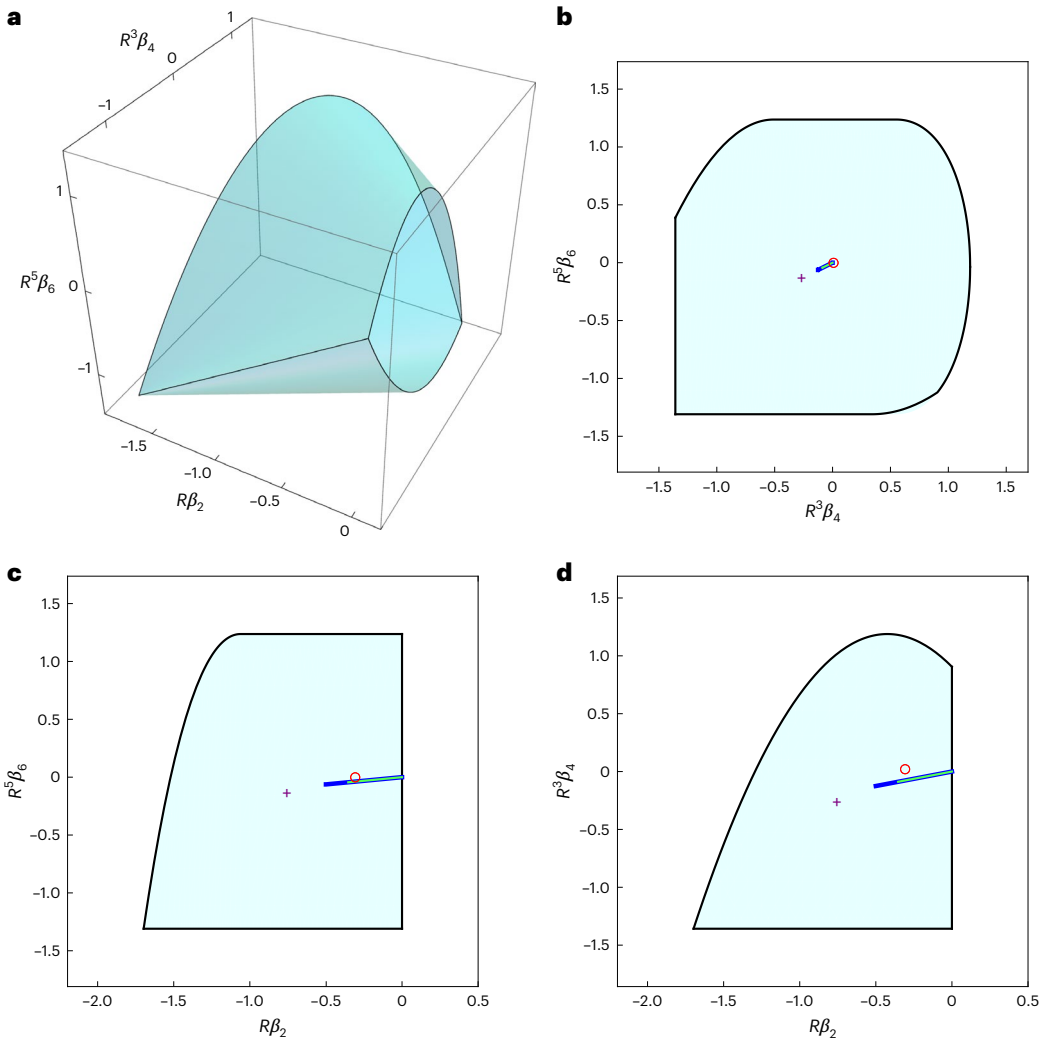

Fig. 1 | Hydrohedron diffusion mode geometry. a, Diffusion mode cross-section of the hydrohedron in the $(R\beta_2, R^3\beta_4, R^5\beta_6)$-hyperplane. **b**–**d**, Its projections to the $(R^3\beta_4, R^5\beta_6)$-plane (**b**), $(R\beta_2, R^5\beta_6)$-plane (**c**) and $(R\beta_2, R^3\beta_4)$-plane (**d**). Causal theories necessarily live inside these shaded regions; choices of transport coefficients in the white region are acausal and excluded. The functions determining the boundaries of each projection (solid black lines) are detailed analytically in the text. The purple crosses represent the location of $\mathcal{N} = 4$ SYM in the holographic regime, the red open circles correspond to conformal kinetic theory in the relaxation time approximation and the green (blue) lines to conformal MIS (conformal BDNK) in the parameter regime where they are causal and linearly stable.

and lower bounded by another piecewise function

$$R^5\beta_6 \geq \begin{cases} -\dfrac{144}{35\pi} & \text{if } -\dfrac{64}{15\pi} \leq R^3\beta_4 < \dfrac{16}{15\pi} \\ -\dfrac{\left[\begin{array}{l} 32,768 + 105\pi R^3\beta_4 \\ \times(32 - 15\pi R^3\beta_4) \end{array}\right]}{8,400\pi} & \text{if } \dfrac{16}{15\pi} \leq R^3\beta_4 \leq \dfrac{128}{45\pi} \\ -\dfrac{\left[\begin{array}{l} 360 + 7\sqrt{30}(34 + 15\pi R^3\beta_4) \\ \times\sqrt{56 - 15\pi R^3\beta_4} \end{array}\right]}{3,150\pi} & \text{if } \dfrac{128}{45\pi} \leq R^3\beta_4 \leq \dfrac{56}{15\pi} \end{cases} . \quad (9)$$

The bounds we outline above, as well as the infinite hierarchy of associated bounds described in 'Diffusion cross-section derivation', are a new set of bounds applying to all theories of relativistic transport exhibiting a diffusion mode of the type in equation (3). The exception is the upper limit of equation (4), which expresses the well-known requirement that the diffusivity D is non-negative, where $D \equiv -\beta_2$. The lower limit of equation (4), for instance, is a new rigorous upper bound on diffusion. For any given theory, measuring or computing the D along with the physical microscopic scale R, the result necessarily lies inside the bound of equation (4) if the theory is causal.

It is of course instructive to consider where known microscopic theories live in this diffusion cross-section. To this end, we show the values of $\{R\beta_2, R^3\beta_4, R^5\beta_6\}$ computed for $\mathcal{N} = 4$ SYM theory using holographic techniques (see also refs. 2,3), conformal kinetic theory in the relaxation time approximation and two phenomenological models: conformal Müller–Israel–Stewart (MIS) theory[22,23], widely adopted in the study of ultrarelativistic nuclear collisions, and the recently introduced conformal Bemfica–Disconzi–Noronha–Kovtun (BDNK) theory[24–27]. These are generic points in the interior of the projected hydrohedron. The exception is that MIS and BDNK intersect the point where $\beta_{2n} = 0$, where the diffusive mode is trivial. It would of course be interesting to identify non-trivial theories that live at the boundaries of the hydrohedron, where theories live in tension with the constraints of causality. In 'Further details on the hydrohedron boundary',

we demonstrate that many of the boundaries (although not all of them) are open, excluding the possibilities of theories living there.

The sound cross-section

In this section, we specialize to a mode defined by the following Taylor series expansion of the dispersion relation

$$\omega(k) = \sum_{n=0}^{\infty} \alpha_{2n+1} k^{2n+1} + \mathrm{i} \sum_{n=1}^{\infty} \beta_{2n} k^{2n} \tag{10}$$

where α_{2n+1} and β_{2n} are real. This includes both sound mode excitations and also Lorentz boosts of the diffusion modes considered in the previous section. Note that for sound waves, α_1 is equal to the speed of sound c_s, whereas β_2 is related to the sound attenuation length Γ_s as $\beta_2 = -\frac{\Gamma_s}{2}$. As before, specializing to modes of the form in equation (10) will give us a cross-section of the full hydrohedron geometry. Note that diffusion is itself a cross-section of sound along the hyperplane defined by $\alpha_{2n+1} = 0$ for all n.

Through the moment problem analysis outlined in 'Sound cross-section derivation', we obtain an infinite set of hierarchical bounds on the transport coefficients $\alpha_{2n+1}, \beta_{2n}$ normalized to the convergence radius R. The first three bounds in this set are

$$|\alpha_1| \leq 1, \tag{11}$$

$$-\frac{16}{3\pi} + \frac{\pi}{2}\alpha_1^2 \leq R\beta_2 \leq 0, \tag{12}$$

$$\frac{128 - 9\pi^2(\alpha_1 - R\beta_2)^2 - 12\pi(\alpha_1 + 2R\beta_2)}{9\pi(-4 + \pi\alpha_1)} \leq R^2\alpha_3 \leq \frac{128 - 9\pi^2(\alpha_1 + R\beta_2)^2 + 12\pi(\alpha_1 - 2R\beta_2)}{9\pi(4 + \pi\alpha_1)}. \tag{13}$$

The first bound in equation (11) expresses the well-known fact that in a causal theory the speed of sound cannot exceed the lightcone speed $v_{LC} = 1$. The remaining two-sided bounds in equations (12) and (13) are new. In particular, if the speed of sound is known, the inequality in equation (12) provides an upper bound for the sound attenuation length Γ_s in units of the convergence radius. For instance, in a d-dimensional conformal field theory, $|\alpha_1| = \frac{1}{\sqrt{d-1}}$ and

$$R\Gamma_s \leq \frac{32}{3\pi} - \frac{\pi}{d-1}. \tag{14}$$

Taken together, the bounds in equations (11)–(13) define a projection of the sound cross-section of the full hydrohedron geometry to the 3D subspace of the first three transport coefficients $\{\alpha_1, R\beta_2, R^2\alpha_3\}$. This projection is a convex shape illustrated in Fig. 2a.

All two-dimensional projections involving pairs of $\{\alpha_1, R\beta_2, R^2\alpha_3\}$ are shown in Fig. 2b–d. The projection to the $(\alpha_1, R\beta_2)$-plane is given by inequalities in equations (11) and (12). As it happened in the diffusion case, the projections to the remaining $(\alpha_1, R^2\alpha_3)$ and $(R\beta_2, R^2\alpha_3)$ planes involve a higher-level inequality (equation (13)) and therefore have more involved explicit expressions. In the $(\alpha_1, R^2\alpha_3)$-plane, we find that the closure of the projection exists within the interval $|\alpha_1| \leq 1$, in which $R^2\alpha_3$ is upper bounded by a piecewise function

$$R^2\alpha_3 \leq \begin{cases} \frac{128 + 3\alpha_1\pi(4 - 3\pi\alpha_1)}{9\pi(4 + \pi\alpha_1)} & \text{if } -1 \leq \alpha_1 < -\frac{4}{3\pi} \\ \frac{4}{\pi} & \text{if } -\frac{4}{3\pi} \leq \alpha_1 < \frac{2}{\pi} \\ \alpha_1\left(3 - \frac{\pi^2}{4}\alpha_1^2\right) & \text{if } \frac{2}{\pi} \leq \alpha_1 \leq 1 \end{cases}, \tag{15}$$

and lower bounded by another piecewise function

$$R^2\alpha_3 \geq \begin{cases} \alpha_1\left(3 - \frac{\pi^2}{4}\alpha_1^2\right) & \text{if } -1 \leq \alpha_1 < -\frac{2}{\pi} \\ -\frac{4}{\pi} & \text{if } -\frac{2}{\pi} \leq \alpha_1 < \frac{4}{3\pi} \\ -\frac{128 - 3\alpha_1\pi(4 + 3\pi\alpha_1)}{9\pi(4 - \pi\alpha_1)} & \text{if } \frac{4}{3\pi} \leq \alpha_1 \leq 1 \end{cases}. \tag{16}$$

For the $(R\beta_2, R^2\alpha_3)$-plane, the closure of the projection exists within the interval $-\frac{16}{3\pi} \leq R\beta_2 \leq 0$, where $R^2\alpha_3$ is upper bounded by a piecewise function

$$R^2\alpha_3 \leq \begin{cases} \frac{(2 - 3\pi R\beta_2)(96 + 18\pi R\beta_2)^{\frac{1}{2}}}{18\pi} & \text{if } -\frac{16}{3\pi} \leq R\beta_2 < -\frac{10}{3\pi} \\ \frac{4}{\pi} & \text{if } -\frac{10}{3\pi} \leq R\beta_2 \leq 0 \end{cases}, \tag{17}$$

and lower bounded by another piecewise function

$$R^2\alpha_3 \geq \begin{cases} -\frac{(2 - 3\pi R\beta_2)(96 + 18\pi R\beta_2)^{\frac{1}{2}}}{18\pi} & \text{if } -\frac{16}{3\pi} \leq R\beta_2 < -\frac{10}{3\pi} \\ -\frac{4}{\pi} & \text{if } -\frac{10}{3\pi} \leq R\beta_2 \leq 0 \end{cases}. \tag{18}$$

In parallel with diffusion case, in Fig. 2 we also provide the values of $\{\alpha_1, R\beta_2, R^2\alpha_3\}$ for $\mathcal{N} = 4$ SYM in the holographic limit, kinetic theory in the relaxation time approximation, MIS and BDNK (the last three also in the conformal regime). Note that $\alpha_1 = \frac{1}{\sqrt{3}}$ in all cases. Again, we find that all of these theories lie at generic points inside the hydrohedron projections, the exception being where MIS and BDNK reach the boundary at $\beta_{2n} = 0$, where the sound mode is that of a perfect conformal fluid.

Furthermore, we note that the sound cross-section has a special corner point. As we demonstrate in 'The stiff fluid facets', when $|\alpha_1| = 1$, all the higher-order transport coefficients vanish and the dispersion relation is uniquely determined:

$$\omega(k) = \pm k. \tag{19}$$

This corresponds to the case of a stiff perfect fluid and fluids boosted to the speed of light, because equation (19) is a fixed point under boosts. The vanishing of the diffusivity for a stiff fluid was also noted recently in ref. 28. Note also that, according to our analysis, $\alpha_1 = \pm 1$ still allows for a range of $R\beta_2$ and $R^2\alpha_3$ values. It is possible that such points may be understood in a limit of a family of dispersion relations where as $\alpha_1 \to \pm 1$, one finds $R \to \infty$ and $\beta_2, \alpha_3 \to 0$ but with the dimensionless products $R\beta_2$ and $R^2\alpha_3$ finite in this limit.

Finally, there are various other physical theories that live at this corner of the hydrohedron, traditionally outside the realm of hydrodynamics, for which our analysis still applies. These include free massless theories and two-dimensional conformal field theories.

Relation to other bounds

We have obtained an infinite class of bounds on transport coefficients. In the literature, there are a number of important bounds on transport that have appeared before. In this section, we comment on the relation to these other bounds.

Perhaps the closest in spirit is that obtained in ref. 29 for a qualitative upper bound on diffusion following from causality considerations

https://doi.org/10.1038/s41567-024-02635-5

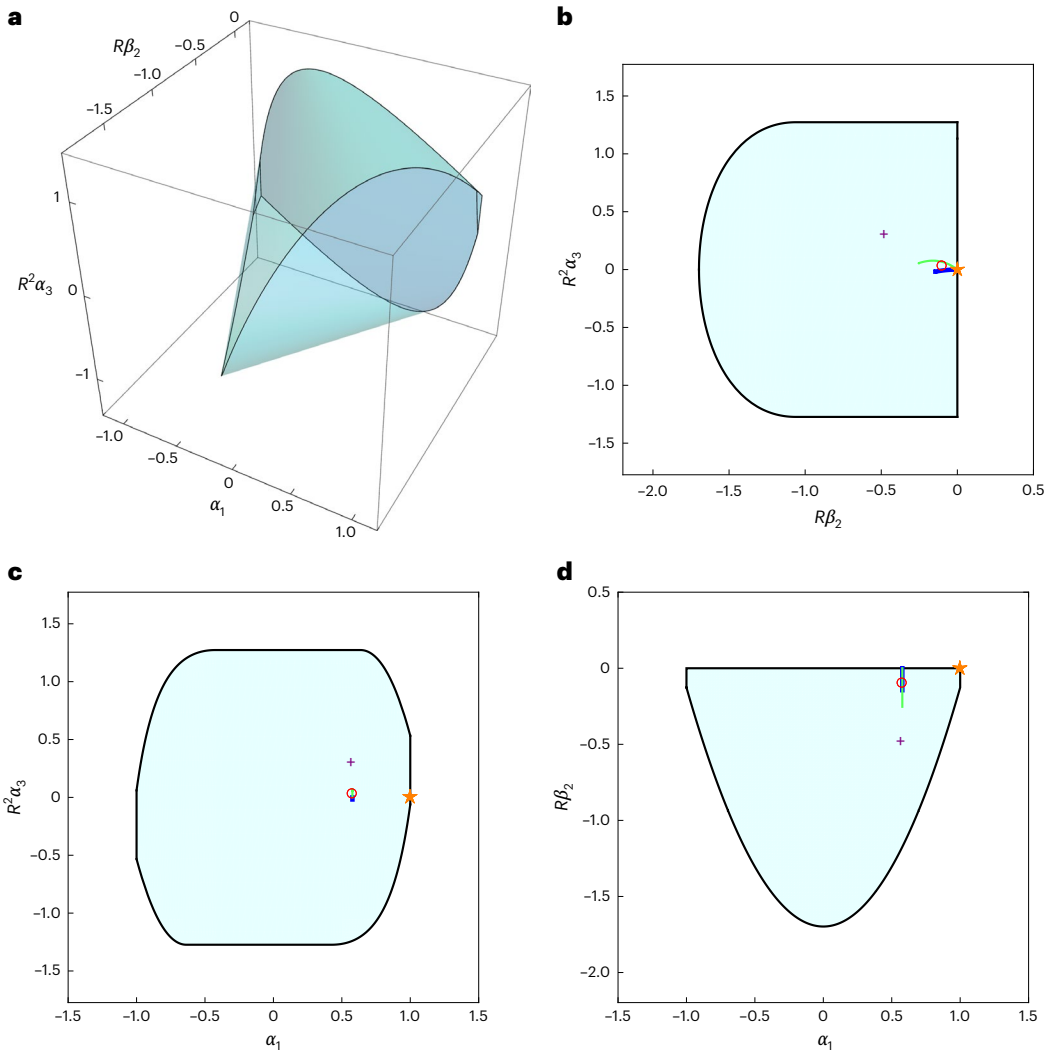

Fig. 2 | Hydrohedron sound mode geometry. a, Sound mode cross-section of the hydrohedron in the $(\alpha 1, R\beta_2, R^2\alpha_3)$-hyperplane. **b**–**d**, Its projections to the $(R\beta_2, R^2\alpha_3)$-plane (**b**), $(\alpha_1, R^2\alpha_3)$-plane (**c**) and $(\alpha_1, R\beta_2)$-plane (**d**). Colour coding as in Fig. 1. The functions determining the boundaries of each projection (solid black lines) are detailed analytically in the text. The purple crosses represent the location of $\mathcal{N} = 4$ SYM in the holographic regime, the red open circles correspond to conformal kinetic theory in the relaxation time approximation, and the green (blue) lines to conformal MIS (conformal BDNK) in the parameter regime where they are causal and linearly stable. Finally, the orange star marks to the special corner point corresponding to the stiff perfect fluid. Note that in these examples, for every triplet $(1/\sqrt{3}, \beta_2, \alpha_3)$, there is a corresponding one $(-1/\sqrt{3}, \beta_2, -\alpha_3)$, which we do not show explicitly for clarity.

$$D \lesssim v^2 \tau_{\mathrm{eq}}, \tag{20}$$

where v is a speed defining a lightcone for operator growth and τ_{eq} is a local equilibration time. This bound was obtained using approximations for the structure of diffusion and gapped modes. This upper bound should be compared with the lower bound in equation (4) in the present work: that is,

$$D \leq \frac{16}{3\pi} v_{\mathrm{LC}} R^{-1} \tag{21}$$

which can be viewed as a rigorous version of equation (20). Recall here that v_{LC} is the lightcone speed. Note that the rigorous version demands that equilibration time is replaced by radius of convergence through $v^2\tau_{\mathrm{eq}} \to v_{\mathrm{LC}} R^{-1}$, and the precise coefficient is determined in equation (21). As we discuss in 'The natural scale of the problem', R and τ_{eq}^{-1} are both characterizations of the scale of non-hydrodynamic physics, and so it is natural that this replacement appears here.

Another notable bound on transport is the KSS bound[20], a conjectured lower bound on viscosity in units of entropy density,

$$\frac{1}{4\pi} \leq \frac{\eta}{s}. \tag{22}$$

We know from string theory considerations[30] that the value of η/s can be lowered below this value, at least perturbatively. We have no direct analogue for this bound. The closest counterpart would be the upper bound in equation (4), in which we conclude that $0 \leq DR$. This illustrates that the KSS bound (or its improved version taking the results of ref. 30 into account) does not follow from causality alone, but, if at all, from other considerations. This is in line with the speed of light v_{LC} not appearing at all in equation (22).

Finally we comment on relations to other Planckian bounds related to KSS, as proposed in refs. 31–34. These are again lower bounds on diffusion, which involve the butterfly velocity v_{B} and the Lyapunov time τ_{L}, for instance

$$v_{\mathrm{B}}^2 \tau_{\mathrm{L}} \lesssim D. \tag{23}$$

Similar comments apply to these bounds; as lower bounds that do not appear in our analysis, it seems unlikely that they are a consequence of the constraints of causality.

Discussion

In this Article, we provide a new look at relativistic hydrodynamics, focusing on constraining the theory as much as possible based on fundamental principles alone. Using microscopic causality, we exclude most of transport coefficient space, leaving a convex geometry in which all causal theories of hydrodynamics necessarily reside. This geometry is uniquely determined from causality alone and thus universal, independent of spacetime dimension, state and any microscopic details. We provide constraints at all orders in the hydrodynamic expansion and present a detailed analysis of the first few orders in the sound and diffusion cross-sections of this geometry.

It is important to note that the hydrohedron is a geometry defined in the space of transport coefficients in units of the momentum scale R, where R is the radius of convergence of the hydrodynamic Taylor series in equation (1). This is an intrinsic scale that may be computed or measured given a specific theory. This may appear an unfamiliar normalization choice, given that the vast majority of previous hydrodynamic literature quotes transport coefficients in units such as temperature or entropy density. However, the universal hydrohedron geometry arises only in units of R. Because in general R is a function of temperature in a way that depends on the theory, if one were to convert units, then the shape would be different between theories and universality would be lost. Indeed, the scale R is the cutoff for the effective theory, marking the breakdown of hydrodynamics where other physical degrees of freedom are required. It is only natural therefore that the universal hydrohedron geometry is apparent when coefficients are normalized by R.

Our analysis did not depend on being in the fluid rest frame. Although our diffusion mode analysis specialized to zero background fluid velocity, applying a boost v to the dispersion relation in equation (3) turns it into the form of a sound mode dispersion relation in equation (10). Transport coefficients can be converted straightforwardly; for the first few orders, $\alpha_1 \to v, \beta_2 \to (1-v^2)^{\frac{3}{2}}\beta_2, \alpha_3 \to 2v(1-v^2)^2\beta_2^2$. The radius of convergence R does not boost in an easily predictable way and requires a microscopic computation in each case. The sound mode results then apply.

We saw that some faces of the hydrohedron were excluded, meaning that the set is open there. Examples are the faces that lie at the boundary of the regions excluded by the moment problem. This is not the case for all faces, however, with the faces $\alpha_1 = \pm 1$ and $\beta_2 = 0$ not following from the moment problem. This raises the interesting possibility of 'distinguished' theories living there, reminiscent of the 3D Ising model in the conformal bootstrap[9]. Indeed, we proved that on the faces $\alpha_1 = \pm 1$, the dispersion relation is uniquely $\omega(k) = \pm k$, which is a stiff perfect fluid. For the face $\beta_2 = 0$, we have found examples of theories that live there, but none that appear to be uniquely determined by low-order transport coefficients (aside from at the intersection with $\alpha_1 = \pm 1$). A family of examples is given by $\omega(k) = 4(1+\mathrm{i})\beta_4\left(\mathrm{i}-1+\sqrt{1+\mathrm{i}k^2}-\mathrm{i}\sqrt{1+k^2}\right)$ for $-1/(4\sqrt{2}) \le \beta_4 \le 0$. It would be interesting to see if there are other geometrically privileged points corresponding to theories of special significance.

Our results use analyticity in two senses. First, the role of equation (2) is simply to exclude singularities from the analytic domain of momentum space Green's functions, which follow directly from the axioms of quantum field theory, as discussed in ref. 7. Second, we required $\omega(k)$ be analytic at $k = 0$, see equation (1): that is, the classical hydrodynamic expansion. However, more is known about the analytic structure of $\omega(k)$ from first principles: for instance, it cannot contain poles[7]. Thus, finding a way to incorporate properties of the 'global' analytic structure of $\omega(k)$—rather than just analyticity at $k = 0$—may result in a more constrained region of transport coefficient space. For instance, a recent conjecture for the analytic structure of chaotic large N thermal two-point functions[35] may have bearing on the analytic structure of $\omega(k)$. Analogously, it is a conjecture in the S-matrix bootstrap programme that the amplitudes are 'maximally analytic' and this conjecture enables stronger constraints; see for example refs. 14,36,37.

This discussion brings us naturally to the problem of including and understanding stochastic fluctuations in this language. In this case, it is known that $\omega(k)$ becomes non-analytic at $k = 0$; see for example ref. 38. These effects arise from nonlinearities treated in perturbation theory: for example, correcting $\omega \to \omega + g\,\delta\omega_{\text{stochastic}} + O(g)^2$, where g is a coupling constant that controls interaction strength. Therefore, as long as the perturbative treatment holds, such corrections can only become important when the causality inequality in equation (2) is saturated, which then imposes that $\Im\mathrm{m}(\delta\omega_{\text{stochastic}}) \le 0$. It would also be interesting to investigate stochastic effects at the level of the Schwinger–Keldysh effective action for hydrodynamics[39–43]. In this context, it seems natural to attempt to lift the techniques presented here to the coefficients that appear in this effective action, instead.

Finally, the methods adopted in our paper can be also used to chart causal convex geometries for other mode types such as Goldstone modes, fast-decaying excitations—such as transient quasinormal modes of holographic black holes—and quasiparticles.

Online content

Any methods, additional references, Nature Portfolio reporting summaries, source data, extended data, supplementary information, acknowledgements, peer review information; details of author contributions and competing interests; and statements of data and code availability are available at https://doi.org/10.1038/s41567-024-02635-5.

References

1. Withers, B. Short-lived modes from hydrodynamic dispersion relations. *J. High Energy Phys.* **06**, 059 (2018).
2. Grozdanov, S., Kovtun, P. K., Starinets, A. O. & Tadić, P. Convergence of the gradient expansion in hydrodynamics. *Phys. Rev. Lett.* **122**, 251601 (2019).
3. Grozdanov, S., Kovtun, P. K., Starinets, A. O. & Tadić, P. The complex life of hydrodynamic modes. *J. High Energy Phys.* **11**, 097 (2019).
4. Abbasi, N. & Tahery, S. Complexified quasinormal modes and the pole-skipping in a holographic system at finite chemical potential. *J. High Energy Phys.* **10**, 076 (2020).
5. Jansen, A. & Pantelidou, C. Quasinormal modes in charged fluids at complex momentum. *J. High Energy Phys.* **10**, 121 (2020).
6. Heller, M. P., Serantes, A., Spaliński, M., Svensson, V. & Withers, B. Convergence of hydrodynamic modes: insights from kinetic theory and holography. *SciPost Phys.* **10**, 123 (2021).
7. Heller, M. P., Serantes, A., Spaliński, M. & Withers, B. Rigorous bounds on transport from causality. *Phys. Rev. Lett.* **130**, 261601 (2023).
8. Rattazzi, R., Rychkov, V. S., Tonni, E. & Vichi, A. Bounding scalar operator dimensions in 4D CFT. *J. High Energy Phys.* **12**, 031 (2008).
9. El-Showk, S. et al. Solving the 3D Ising model with the conformal bootstrap. *Phys. Rev. D* **86**, 025022 (2012).
10. Simmons-Duffin, D. The conformal bootstrap. In *Proc. Theoretical Advanced Study Institute in Elementary Particle Physics* (eds Polchinski, J. et al.) 1–74 (World Scientific, 2017).
11. Poland, D., Rychkov, S. & Vichi, A. The conformal bootstrap: theory, numerical techniques, and applications. *Rev. Mod. Phys.* **91**, 015002 (2019).
12. Arkani-Hamed, N., Huang, T.-C. & Huang, Y.-t. The EFT-hedron. *J. High Energy Phys.* **05**, 259 (2021).
13. Caron-Huot, S., Li, Y. Z., Parra-Martinez, J. & Simmons-Duffin, D. Causality constraints on corrections to Einstein gravity. *J. High Energ. Phys.* **2023**, 122 (2023).
14. Kruczenski, M., Penedones, J. & van Rees, B. C. Snowmass white paper: S-matrix bootstrap. Preprint at https://arxiv.org/abs/2203.02421 (2022).

15. de Rham, C., Kundu, S., Reece, M., Tolley, A. J. & Zhou, S.-Y. Snowmass white paper: UV constraints on IR physics. Preprint at https://doi.org/10.48550/arXiv.2203.06805 (2022).
16. Carrillo Gonzalez, M., de Rham, C., Pozsgay, V. & Tolley, A. J. Causal effective field theories. *Phys. Rev. D* **106**, 105018 (2022).
17. Bellazzini, B., Elias Miró, J., Rattazzi, R., Riembau, M. & Riva, F. Positive moments for scattering amplitudes. *Phys. Rev. D* **104**, 036006 (2021).
18. Schmüdgen, K. Ten lectures on the moment problem. Preprint at https://arXiv.org/abs/2008.12698 (2020).
19. Schmüdgen, K. et al. *The Moment Problem* (Springer, 2017).
20. Kovtun, P., Son, D. T. & Starinets, A. O. Viscosity in strongly interacting quantum field theories from black hole physics. *Phys. Rev. Lett.* **94**, 111601 (2005).
21. Caron-Huot, S. & Van Duong, V. Extremal effective field theories. *J. High Energy Phys.* **05**, 280 (2021).
22. Muller, I. Zum Paradoxon der Warmeleitungstheorie. *Z. Phys.* **198**, 329–344 (1967).
23. Israel, W. & Stewart, J. M. Transient relativistic thermodynamics and kinetic theory. *Annals Phys.* **118**, 341–372 (1979).
24. Bemfica, F. S., Disconzi, M. M. & Noronha, J. Causality and existence of solutions of relativistic viscous fluid dynamics with gravity. *Phys. Rev. D* **98**, 104064 (2018).
25. Bemfica, F. S., Disconzi, M. M. & Noronha, J. Nonlinear causality of general first-order relativistic viscous hydrodynamics. *Phys. Rev. D* **100**, 104020 (2019); e rratum **105**, 069902 (2022).
26. Bemfica, F. S., Disconzi, M. M. & Noronha, J. First-order general-relativistic viscous fluid dynamics. *Phys. Rev. X* **12**, 021044 (2022).
27. Kovtun, P. First-order relativistic hydrodynamics is stable. *J. High Energy Phys.* **10**, 034 (2019).
28. Gavassino, L. Bounds on transport from hydrodynamic stability. *Phys. Lett. B* **840**, 137854 (2023).
29. Hartman, T., Hartnoll, S. A. & Mahajan, R. Upper bound on diffusivity. *Phys. Rev. Lett.* **119**, 141601 (2017).
30. Buchel, A., Myers, R. C. & Sinha, A. Beyond eta/s = 1/4 pi. *J. High Energy Phys.* **03**, 084 (2009).
31. Hartnoll, S. A. Theory of universal incoherent metallic transport. *Nature Phys.* **11**, 54 (2015).
32. Blake, M. Universal charge diffusion and the butterfly effect in holographic theories. *Phys. Rev. Lett.* **117**, 091601 (2016).
33. Blake, M. Universal diffusion in incoherent black holes. *Phys. Rev. D* **94**, 086014 (2016).
34. Hartnoll, S. A. & Mackenzie, A. P. Colloquium: Planckian dissipation in metals. *Rev. Mod. Phys.* **94**, 041002 (2022).
35. Dodelson, M., Iossa, C., Karlsson, R. & Zhiboedov, A. A thermal product formula. *J. High Energ. Phys.* **2024**, 36 (2024).
36. Paulos, M. F., Penedones, J., Toledo, J., van Rees, B. C. & Vieira, P. The S-matrix bootstrap. Part III: higher dimensional amplitudes. *J. High Energy Phys.* **12**, 040 (2019).
37. Correia, M., Sever, A. & Zhiboedov, A. An analytical toolkit for the S-matrix bootstrap. *J. High Energy Phys.* **03**, 013 (2021).
38. Kovtun, P. Lectures on hydrodynamic fluctuations in relativistic theories. *J. Phys. A* **45**, 473001 (2012).
39. Haehl, F. M., Loganayagam, R. & Rangamani, M. The fluid manifesto: emergent symmetries, hydrodynamics, and black holes. *J. High Energy Phys.* **01**, 184 (2016).
40. Crossley, M., Glorioso, P. & Liu, H. Effective field theory of dissipative fluids. *J. High Energy Phys.* **09**, 095 (2017).
41. Jensen, K., Pinzani-Fokeeva, N. & Yarom, A. Dissipative hydrodynamics in superspace. *J. High Energy Phys.* **09**, 127 (2018).
42. Haehl, F. M., Loganayagam, R. & Rangamani, M. Effective action for relativistic hydrodynamics: fluctuations, dissipation, and entropy inflow. *J. High Energy Phys.* **10**, 194 (2018).
43. Liu, H. & Glorioso, P. Lectures on non-equilibrium effective field theories and fluctuating hydrodynamics. *PoS* **TASI2017**, 008 (2018).

Methods

The moment problem

Diffusion cross-section derivation. A general diffusive mode can be written as the Taylor series in equation (3). Inserting equation (3) into equation (2) with $k = re^{i\theta}$ and taking the $r \to 0$ limit at $\theta = 0$, it immediately follows[7]

$$\beta_2 \leq 0. \tag{24}$$

If $\beta_2 = 0$, then $\beta_4 \leq 0$ also, and so on in this fashion.

To obtain additional bounds on transport, we may multiply equation (2) by any non-negative periodic function of θ, $\tilde{p}(\theta)$ and integrate around a circle of radius $r < R$,

$$\int_0^{2\pi} \tilde{p}(\theta)\tilde{\mu}(\theta)d\theta \geq 0, \qquad \tilde{\mu}(\theta) \equiv \frac{|\Im\mathfrak{m}\, k| - \Im\mathfrak{m}\, \omega(k)}{|k|}, \tag{25}$$

or, more conveniently for $x = \cos\theta$,

$$\int_{-1}^{1} p(x)\mu(x)dx \geq 0, \quad \mu(x) \equiv 1 - \sum_{n=1}^{\infty} r^{2n-1}\beta_{2n}(1-x^2)^{-\frac{1}{2}}T_{2n}(x), \tag{26}$$

where $T_n(x)$ are Chebyshev polynomials of the first kind. Given some $p(x)$, the left-hand side of equation (26) evaluates to a sum of transport coefficients, revealing a bound. Assembling all such bounds, one can then carve out regions of excluded parameter space by considering all $r < R$.

An analogous construction in the context of scattering amplitudes is discussed in ref. 17 utilizing the theory of moments, an efficient route to generate optimal bounds, which we adopt here. Because $\mu(x) = \mu(-x)$, we restrict our attention to even functions of x. Then, the condition in equation (26) becomes a condition on the matrices of moments of the measure $\mu(x)dx$. In particular, at a given N, we construct the following Hankel matrices of the moments of this measure[17,18]:

$$(H_N^{\ell})_{ij} = a_{i+j+\ell}, \quad i,j = 0,\ldots,\left\lfloor\frac{N-\ell}{2}\right\rfloor, \qquad a_n \equiv \frac{1}{2}\int_{-1}^{1} x^{2n}\mu(x)dx, \tag{27}$$

in which i and j are the indices of the Hankel matrix and ℓ is a label of such a matrix, and then equation (26) is the condition that the following matrices are positive semidefinite:

$$H_N^0 \succcurlyeq 0, \quad H_N^1 \succcurlyeq 0, \quad H_{N-1}^0 - H_N^1 \succcurlyeq 0, \quad H_{N-1}^1 - H_N^2 \succcurlyeq 0. \tag{28}$$

The moments a_n are related to β_{2n} (equation (26)) through

$$a_n = \frac{1}{2n+1} - 2^{-(2n+1)}\pi\sum_{j=1}^{n}\binom{2n}{n-j}r^{2j-1}\beta_{2j}, \tag{29}$$

$$r^{2n-1}\beta_{2n} = \frac{4}{\pi(1-4n^2)} - \frac{4}{\pi}\sum_{j=0}^{n}\sum_{q=0}^{j}(-1)^{j-q}\binom{2n}{2j}\binom{j}{q}a_{n-j+q}, \tag{30}$$

and thus, given N, the conditions of positive semidefinite Hankel matrices translate into bounds on a subset of transport coefficients. Here we consider the constraints arising from the $N = 2$ and $N = 3$ moment problems and thus construct the projections of the hydrohedron into parameter space spanned by the transport coefficients $\{R\beta_2, R^3\beta_4, R^5\beta_6\}$ described earlier.

$N = 2$ case. In this case, we require positive semidefiniteness of the following matrices for all $r < R$:

$$H_2^0 = \begin{pmatrix} 1 & \frac{1}{3} - \frac{\pi}{8}r\beta_2 \\ \frac{1}{3} - \frac{\pi}{8}r\beta_2 & \frac{1}{5} - \frac{\pi}{8}r\beta_2 - \frac{\pi}{32}r^3\beta_4 \end{pmatrix},$$
$$H_2^1 = \left(\frac{1}{3} - \frac{\pi}{8}r\beta_2\right), \quad H_1^0 - H_2^1 = \left(\frac{2}{3} + \frac{\pi}{8}r\beta_2\right), \tag{31}$$
$$H_1^1 - H_2^2 = \left(\frac{2}{15} + \frac{\pi}{32}r^3\beta_4\right).$$

These conditions, together with the inequality in equation (24), lead to the inequalities in equations (4) and (5).

It is straightforward to demonstrate that the non-excluded region defined by inequalities in equations (4) and (5) is not closed. For example, at $\beta_2 = 0$ we have that $\beta_4 \leq 0$, and thus a portion of the $\beta_2 = 0$ boundary indicated in Fig. 1d is excluded. It can be established that the quadratic portion of this boundary as well as the line $\beta_4 = -\frac{64}{15\pi}$ are also excluded. At these loci in the $(R\beta_2, R^3\beta_4)$-plane, considering the constraint in equation (2) at $r = R$ uniquely fixes all higher-order transport coefficients. This leads to dispersion relations that feature poles and hence violate the causality condition in equation (2) (see ref. 7), thus showing that loci where the first inequality in equation (5) is saturated do not belong to the hydrohedron. An example of such dispersion relation at $\beta_4 = -64/15\pi$ is

$$\tilde{w}(\tilde{k}) = -\frac{2\mathrm{i}}{\pi}\left(\left(\tilde{k} - \tilde{k}^{-1}\right)\operatorname{arctanh}\tilde{k} + \frac{1 - 2(1-2a_1)\tilde{k}^2 + \tilde{k}^4}{1-\tilde{k}^4}\right) \tag{32}$$

with $k = R\tilde{k}$, $\omega = R\tilde{w}$ and $a_1 = \frac{1}{3} - \frac{\pi}{8}\beta_2 \in [1/3, 1]$ parameterizing the curve in the projection plane. Further details may be found in 'Further details on the hydrohedron boundary'.

$N = 3$ case. $H_3^0 \succcurlyeq 0$ and $H_2^1 - H_3^2 \succcurlyeq 0$ give no new constraints beyond those in equation (5), whereas $H_2^0 - H_3^1 \succcurlyeq 0$ and $H_3^1 \succcurlyeq 0$ respectively, for all $r < R$, give the additional bounds in equation (6).

We note that when $R^5\beta_6$ saturates any of the inequalities in equation (6), both $R^5\beta_6$ and all the higher-order transport coefficients are fixed in terms of $R\beta_2$ and $R^3\beta_4$. The resulting dispersion relations are excluded due to the presence of poles ('Further details on the hydrohedron boundary'). As a consequence, the loci where equation (6) is saturated do not belong to the hydrohedron.

Sound cross-section derivation. The dispersion relation of a sound mode has the Taylor series representation in equation (10). The bound on the speed of sound in equation (11) is obtained by considering the fundamental inequality in equation (2) at $\theta = \pi/2$ in the $r \to 0$ limit[7]. As happened in the diffusion case, to find the remaining ones, the optimal way to proceed is translating the causality condition in equation (2) into a moment problem. This time, however, the relevant moment problem is a trigonometric one formulated on the circle $\theta \in [0, 2\pi)$. We work with the following unit-normalized density

$$\mu(\theta) \equiv \left.\frac{|\Im\mathfrak{m}k| - \Im\mathfrak{m}\omega(k)}{4|k|}\right|_{k=re^{i\theta}}, \tag{33}$$

and consider the moments

$$\gamma_n \equiv \int_0^{2\pi} e^{-in\theta}\mu(\theta)d\theta, \quad n = 0, \pm1, \pm2, \ldots, \tag{34}$$

which satisfy $\gamma_{-n} = \gamma_n^*$, and read

$$\gamma_0 = 1, \quad \gamma_{2n+1} = \mathrm{i}\frac{\pi}{4}r^{2n}\alpha_{2n+1}, \quad \gamma_{2n} = -\frac{1}{(4n^2-1)} - \frac{\pi}{4}r^{2n-1}\beta_{2n}, \quad n \geq 0. \tag{35}$$

Our focus will be on the following Toeplitz matrices:

$$(T_N)_{ij} \equiv \gamma_{j-i}, \quad i,j = 0,1,\ldots,N \tag{36}$$

The reason is that $\{\gamma_n\}_{n=0}^N$ is a sequence of moments if and only if T_N is positive semidefinite, $T_N \succcurlyeq 0$ (ref. 19). We now discuss the consequences of this theorem for the transport coefficients in the $N = 1, 2, 3$ cases.

$N = 1$ case. The Toeplitz matrix is given by

$$T_1 = \begin{pmatrix} 1 & \mathrm{i}\frac{\pi}{4}\alpha_1 \\ -\mathrm{i}\frac{\pi}{4}\alpha_1 & 1 \end{pmatrix}. \tag{37}$$

This matrix is positive semidefinite provided that $\det T_1 \geq 0$. This condition results in the two-sided bound $|\alpha_1| \leq \frac{4}{\pi}$, which is less sharp than equation (11) and therefore superseded by it.

N = 2 case. The Toeplitz matrix is given by

$$T_2 = \begin{pmatrix} 1 & \mathrm{i}\frac{\pi}{4}\alpha_1 & -\frac{1}{3} - \frac{\pi}{4}r\beta_2 \\ -\mathrm{i}\frac{\pi}{4}\alpha_1 & 1 & \mathrm{i}\frac{\pi}{4}\alpha_1 \\ -\frac{1}{3} - \frac{\pi}{4}r\beta_2 & -\mathrm{i}\frac{\pi}{4}\alpha_1 & 1 \end{pmatrix}. \tag{38}$$

Together with equation (4), the requirement that $T_2 \geqslant 0$ gives rise to the two-sided inequality in equation (12).

In the case where $R\beta_2$ saturates the lower bound in equation (12), all the higher-order transport coefficients are also fixed uniquely in terms of α_1. The associated dispersion relation features poles and is therefore excluded. This shows that the curve $R\beta_2 = -\frac{16}{3\pi} + \frac{\pi}{2}\alpha_1^2, |\alpha_1| \leq 1$ does not belong to the hydrohedron. We refer the reader to 'Further details on the hydrohedron boundary' for additional details.

N = 3 case. The positive semidefiniteness of T_3 leads to the two-sided bound in equation (13).

As happened in the $N = 2$ case, the loci where any side of the bound in equation (13) is saturated are outside the hydrohedron. The reason is as before: at these boundaries, $R^2\alpha_3$ and all the higher-order transport coefficients are fixed uniquely in terms of α_1 and $R\beta_2$, leading to a dispersion relation that features poles and is thus in conflict with the causality condition in equation (2).

Further details on the hydrohedron boundary

Diffusion. Here we explain why the boundaries of the diffusion cross-section of the hydrohedron determined by the moment problem are open. These boundaries have a different status than the ones associated to the condition $R\beta_2 \leq 0$; in principle, this second kind of boundary can contain dispersion relations that uphold equation (2) and thus belong to the hydrohedron. The analysis that follows relies essentially on standard results in the moment problem literature[18,19].

We start by defining the moment cone $\mathcal{S}_{m+1}$ as the set of all truncated moment sequences of length $m+1$ of all Radon measures in $[0,1]$ (the latter set being denoted as $M_+([0,1])$): that is,

$$\mathcal{S}_{m+1} \equiv \left\{ s = (a_0, a_1, \dots, a_m) \,:\, a_j = \int_0^1 x^j d\mu(x), j = 0, \dots, m, \mu \in M_+([0,1]) \right\}, \tag{39}$$

and point out that every non-trivial moment sequence $s \in \mathcal{S}_{m+1}$ can be represented by a measure of the form

$$\mu = \sum_{j=1}^{p} m_j \delta_{x_j}, \quad p \leq m+1, \tag{40}$$

with pairwise distinct roots $x_j \in [0,1]$, weights $m_j > 0$ for all j, and δ_{x_j} a Dirac measure at the point x_j. A central quantity in our analysis is the index of this representing measure, $\mathrm{ind}(\mu)$, defined as

$$\mathrm{ind}\,(\mu) \equiv \sum_{j=1}^{p} \epsilon(x_j), \quad \text{where} \quad \epsilon(0) = \epsilon(1) = 1 \quad \text{and} \quad \epsilon(x) = 2 \quad \text{for} \quad x \in (0,1), \tag{41}$$

with $\mathrm{ind}(s)$ denoting the minimal index of all representing measures of s.

The crucial result is Theorem 10.7 in ref. 19 (Theorem 3.5 in ref. 18). Among others, in this theorem the following statements are shown to be equivalent:

(1) $s \in \partial\mathcal{S}_{m+1}$
(2) $\mathrm{ind}(s) \leq m$
(3) The representing measure is unique

From this result, it follows that the moment sequences lying at the boundary of the moment cone are of the form

$$a_0 = \sum_{j=1}^{p} m_j = 1, \quad a_n = \sum_{j=1}^{p} m_j x_j^n, \quad n > 0. \tag{42}$$

From the expression above, the inversion formula in equation (30) entails that

$$\tilde{w}(\tilde{k}) = -\frac{2\mathrm{i}}{\pi}\left(1 + \left(\tilde{k} - \frac{1}{\tilde{k}}\right)\operatorname{arctanh}\tilde{k} - \sum_{j=1}^{p} m_j \frac{2\tilde{k}^2\left(1 - 2x_j + \tilde{k}^2\right)}{\left(1 + \tilde{k}^2\right)^2 - 4x_j\tilde{k}^2}\right). \tag{43}$$

These dispersion relations are associated to the boundaries of the moment cones and uniquely determined by the relevant set of weights m_j and roots x_j. They feature poles at locations fixed by x_j; hence, as shown in ref. 7, they do not respect the causality condition in equation (2) everywhere in the complex k-plane and thus do not belong to the hydrohedron. This shows the main result of this subsection: that the boundaries of the diffusion cross-section of hydrohedron determined by the moment problem are open. We reiterate that this analysis does not apply to the other boundaries, prescribed by the $R\beta_2 \leq 0$ condition.

With the main result established, we now specialize the general discussion above to the cases $m = 1, 2, 3$ for the interested reader.

m = 1 case. We have that $\mathrm{ind}(s) = 1$, and hence there is a single root $x_1 \in \{0, 1\}$ and weight $m_1 = 1$. The case $x_1 = 0$ leads to $R\beta_2 = \frac{8}{3\pi}$ and is unphysical. We are left with the case where $x_1 = 1$, resulting in a moment sequence of the form $a_{n\geq 0} = 1$. Upon using equation (30), one finds that this boundary point saturates all the lower bounds on c_{2n} put forward in ref. 7, when specialized to a purely diffusive mode.

m = 2 case. The new cases have $\mathrm{ind}(s) = 2$ and correspond to

(i) $p = 1, m_1 = 1$ and $x_1 \equiv x \in (0,1)$ but otherwise free and
(ii) $p = 2, x_1 = 0, x_2 = 1, m_1 = 1 - \alpha$ and $m_2 = \alpha$ with $\alpha \in (0,1)$.

In case (i), the moment sequence takes the form $a_{n\geq 0} = x^n$. With the help of equation (29), one can easily show that this form implies that $R^3\beta_4$ saturates the upper bound in the first inequality of equation (5), with x a parameter labelling points on this boundary.

In case (ii), the moment sequence takes the form $a_0 = 1, a_{n>0} = \alpha$. It can be readily checked that the relations above imply that $R^3\beta_4 = -\frac{64}{15\pi}$, such that the lower bound in the first inequality of equation (5) is saturated, with α labelling points on this boundary. The choice of weights and roots for case (ii) gives back the dispersion relation in equation (32) in 'Diffusion cross-section derivation' upon usage of equation (43).

We conclude by pointing out that there is a fundamental difference between the dispersion relations associated to cases (i) and (ii). Although both feature poles and hence violate in equation (2) somewhere in the complex k-plane, the region where equation (2) is violated includes part of the unit disk for the former but not for the latter. Note that this also means the transport coefficients from (i) do not form part of the closure of the hydrohedron, whilst transport coefficients from (ii) do.

m = 3 case. The new cases have ind(*s*) = 3. They are

(iii) $p = 2, x_1 = 0, x_2 = x \in (0,1), m_1 = 1-\alpha, m_2 = \alpha$ with $\alpha \in (0,1)$ and
(iv) $p = 2, x_1 = x \in (0,1), x_2 = 1, m_1 = \alpha, m_2 = 1-\alpha$ with $\alpha \in (0,1)$.

For case (iii), the moment sequence is given by $a_0 = 1$, $a_{n>0} = \alpha x^n$. This relation, together with equation (29), implies that $R^5\beta_6$ saturates the upper bound given in equation (6). For case (iv), $a_{n\geq 0} = \alpha x^n + (1-\alpha)$, from which it follows that $R^5\beta_6$ saturates the lower bound given in equation (6). The dispersion relations associated with cases (iii) and (iv) can be readily found using equation (43). Both feature poles and are therefore discarded, implying that the boundaries of the hydrohedron set by equation (6) are open.

Sound. As discussed in 'Sound cross-section derivation', the relevant moment problem for the sound geometry is a trigonometric one. In this case, the mathematical results necessary for our analysis can be found in Chapter 11 of ref. 19.

For the truncated trigonometric moment problem, the moment cone $\mathcal{S}_{m+1}$ is defined as the set of all moment sequences of length $n+1$ associated to all Radon measures on the unit circle $\mathbb{T}$ (the latter set being denoted as $M_+(\mathbb{T})$),

$$\mathcal{S}_{m+1} \equiv \left\{ s = (\gamma_0, \gamma_1, \ldots, \gamma_n) : \gamma_j = \int_{\mathbb{T}} z^{-j} d\mu(z),\ \mu \in M_+(\mathbb{T}) \right\}. \tag{44}$$

A sequence s belonging to the boundary of $\mathcal{S}_{m+1}$ has a unique representing measure supported on at most m points. From this result, it follows that if $s \in \partial\mathcal{S}_{m+1}$, then

$$\gamma_n = \sum_{j=1}^{p} m_j e^{-in\theta_j}, \quad \theta_j \in [0, 2\pi) \tag{45}$$

and $p \leq m$. We now explore the consequences of this assertion for the cases $m = 2, 3$. We do not consider the $m = 1$ case because it is beyond the stiff fluid facets we discuss in 'The stiff fluid facets'.

m = 2 case. The moment sequence is of the form $\gamma_n = \frac{1}{2}\left(e^{-in\theta} + e^{-in(\pi-\theta)}\right)$. This expression implies that $R\beta_2$ saturates the lower bound in equation (12). Upon using equations (35) and (1), this moment sequence results in the dispersion relation

$$\tilde{w}(\tilde{k}) = -\frac{2i}{\pi}\left((\tilde{k} - \tilde{k}^{-1})\ \mathrm{arctanh}\ (\tilde{k}) + \frac{1-\tilde{k}^4}{1-2\cos(2\theta)\tilde{k}^2+\tilde{k}^4}\right) - \frac{4\sin(\theta)}{\pi}\frac{\tilde{k}(1+\tilde{k}^2)}{1-2\cos(2\theta)\tilde{k}^2+\tilde{k}^4}, \tag{46}$$

with $\sin(\theta) = -\frac{\pi}{4}\alpha_1$. This dispersion relation does not belong to the hydrohedron: it features poles, and moreover it does not belong to its closure, because it also violates equation (2) in the vicinity of $k^2 = 1$ inside the unit disk.

m = 3 case. The representing measure has three support points. There are two candidate moment sequences such that γ_{2n+1} is purely imaginary and γ_{2n} purely real, $\gamma_n^{(\pm)} = \alpha\left(e^{-in\theta} + e^{-in(\pi-\theta)}\right) + (1-2\alpha)e^{\pm\frac{in\pi}{2}}$. For $\gamma_n^{(+)}$, $R^2\alpha_3$ saturates the lower bound in equation (13); for $\gamma_n^{(-)}$, it saturates the upper bound on the same equation. The dispersion relations associated with $\gamma_n^{(+)}$ and $\gamma_n^{(-)}$ are, respectively,

$$\tilde{w}^{(+)}(\tilde{k}) = -\frac{2i}{\pi}\left((\tilde{k} - \tilde{k}^{-1})\ \mathrm{arctanh}\ \tilde{k} + \frac{(1-\tilde{k}^2)(1-2(\cos(2\theta)-4\alpha\cos(\theta)^2)\tilde{k}^2+\tilde{k}^4)}{(1+\tilde{k}^2)(1-2\cos(2\theta)\tilde{k}^2+\tilde{k}^4)}\right) + \frac{4}{\pi}\tilde{k}\frac{1-2\alpha}{1+\tilde{k}^2} - \frac{8}{\pi}\tilde{k}\frac{\alpha\sin(\theta)(1+\tilde{k}^2)}{1-2\cos(2\theta)\tilde{k}^2+\tilde{k}^4}, \tag{47}$$

$$\tilde{w}^{(-)}(\tilde{k}) = -\frac{2i}{\pi}\left((\tilde{k} - \tilde{k}^{-1})\ \mathrm{arctanh}\ \tilde{k} + \frac{(1-\tilde{k}^2)(1-2(\cos(2\theta)-4\alpha\cos(\theta)^2)\tilde{k}^2+\tilde{k}^4)}{(1+\tilde{k}^2)(1-2\cos(2\theta)\tilde{k}^2+\tilde{k}^4)}\right) - \frac{4}{\pi}\tilde{k}\frac{1-2\alpha}{1+\tilde{k}^2} - \frac{8}{\pi}\tilde{k}\frac{\alpha\sin(\theta)(1+\tilde{k}^2)}{1-2\cos(2\theta)\tilde{k}^2+\tilde{k}^4}. \tag{48}$$

As mentioned earlier, both feature poles and are in conflict with the causality condition (2).

The stiff fluid facets

Given the sound mode dispersion relation in equation (10) with luminal sound speed $\alpha_1 = \pm 1$, the causality condition in equation (2) uniquely fixes the dispersion relation to be $\omega(k) = \pm k$. To prove this, first note that

$$|\mathfrak{Im}\, k| - \mathfrak{Im}\, \omega(k) = |r\sin\theta| - \sum_{n=0}^{\infty}\alpha_{2n+1}r^{2n+1}\sin\left((2n+1)\theta\right) - \sum_{n=1}^{\infty}\beta_{2n}r^{2n}\cos\left(2n\theta\right). \tag{49}$$

By equation (2), this must be non-negative for all $0 \leq r < R$ and $0 \leq \theta < 2\pi$ (for $r \geq R$, the Taylor series representation is invalid). Taking $\alpha_1 = 1$ and restricting to $\theta \in [0, \pi]$ gives a cancellation between the first two terms in this r expansion:

$$|\mathfrak{Im}\, k| - \mathfrak{Im}\, \omega(k) = -\sum_{n=1}^{\infty}\alpha_{2n+1}r^{2n+1}\sin\left((2n+1)\theta\right) - \sum_{n=1}^{\infty}\beta_{2n}r^{2n}\cos\left(2n\theta\right). \tag{50}$$

Thus the leading term in this expansion is now at order r^2. Let us proceed by induction. Take all coefficients up to order r^{m-1} to be zero, with the exception of α_1, and note that $m \geq 2$. If m is even, then the next term in the expansion gives the constraint (in the limit $r \to 0$)

$$-\beta_{m/2}\cos(m\theta) \geq 0, \qquad \forall\theta \in [0,\pi] \tag{51}$$

and hence $\beta_{m/2} = 0$. If instead m is odd, then the next term in the expansion gives the constraint (in the limit $r \to 0$)

$$-\alpha_{(m-1)/2}\sin(m\theta) \geq 0, \qquad \forall\theta \in [0,\pi] \tag{52}$$

and thus, similarly, $\alpha_{(m-1)/2} = 0$. Hence all coefficients zero up to order r^{m-1} implies the coefficients at order r^m are zero. Finally, we note that the base case $m = 2$ is covered by the above analysis, $\beta_2 = 0$, which completes the proof for $\alpha_1 = 1$. The proof for $\alpha_1 = -1$ proceeds analogously. We note the observation that $\alpha_1 = \pm 1 \Rightarrow \beta_2 = 0$ was also given in ref. 28.

Data availability

No data are required to interpret, verify or extend the research in this article.

Acknowledgements

We thank F. Haehl and S. Hartnoll for discussions. A.S. acknowledges financial support from grant no. CEX2019-000918-M funded by Ministerio de Ciencia e Innovación (MCIN)/Agencia Estatal de Investigación (AEI)/10.13039/501100011033. M.S. is supported by the National Science Centre, Poland, under grant no. 2021/41/B/ST2/02909. B.W. is supported by a Royal Society University Research Fellowship and in part by the Science and Technology Facilities Council (Consolidated Grant 'Exploring the Limits of the Standard Model and Beyond'). This project has received funding from the European Research Council (ERC) under the European Union's Horizon 2020 research and innovation

programme (grant no. 101089093/project acronym: High-TheQ/PI: M.P.H.). Views and opinions expressed are however those of the authors only and do not necessarily reflect those of the European Union or the European Research Council. Neither the European Union nor the granting authority can be held responsible for them. Published OA with partial support from the Belgian University Foundation.

Author contributions

B.W. conceived this research. A.S. and B.W. implemented and executed the moments problem. M.P.H. and M.S. contributed to the interpretation of the results. The manuscript was written with contributions and insights from all the authors.

Competing interests

The authors declare no competing interests.

Additional information

Correspondence and requests for materials should be addressed to Michal P. Heller.

Peer review information *Nature Physics* thanks Takato Yoshimura and the other, anonymous, reviewer(s) for their contribution to the peer review of this work.